

Cross sections for α -particle induced reactions on $^{115,116}\text{Sn}$ around the Coulomb barrier

D. Filipescu,^{1,*} V. Avrigeanu,¹ T. Glodariu,¹ C. Mihai,¹ D. Bucurescu,¹ M. Ivaşcu,¹ I. Căta-Danil,¹ L. Stroe,¹ O. Sima,² G. Căta-Danil,³ D. Deleanu,¹ D. G. Ghiţă,¹ N. Mărginean,¹ R. Mărginean,¹ A. Negret,¹ S. Pascu,¹ T. Sava,¹ G. Suliman,¹ and N. V. Zamfir¹

¹“Horia Hulubei” National Institute for Physics and Nuclear Engineering, P.O. Box MG-6, 077125 Bucharest-Magurele, Romania

²Nuclear Physics Department, University of Bucharest, Bucharest, Romania

³Physics Department, University Politehnica of Bucharest, Bucharest, Romania

(Received 23 December 2010; published 20 June 2011)

The cross sections of the $^{115}\text{Sn}(\alpha,\gamma)^{119}\text{Te}$, $^{115}\text{Sn}(\alpha,n)^{118}\text{Te}$, and $^{116}\text{Sn}(\alpha,n)^{119}\text{Te}$ reactions (both on ground and isomeric states) have been measured at effective center-of-mass energies from 9.3 to 14.8 MeV. During a first experiment, enriched self-supporting ^{115}Sn (51.2%) + ^{116}Sn (24.4%) foils were bombarded with an α beam delivered by the Bucharest IFIN-HH Tandem Accelerator. In a second experiment, a highly enriched ^{116}Sn target was irradiated in order to disentangle the experimental cross section contributions due to $^{115}\text{Sn}(\alpha,\gamma)^{119}\text{Te}$ and $^{115}\text{Sn}(\alpha,n)^{118}\text{Te}$ reactions obtained in the first measurement. The beam-induced activity was measured with two large volume HPGe detectors in close geometry. The experimental results were compared with theoretical predictions obtained in the framework of the statistical model.

DOI: [10.1103/PhysRevC.83.064609](https://doi.org/10.1103/PhysRevC.83.064609)

PACS number(s): 25.55.-e, 27.60.+j, 26.30.-k, 24.60.-k

I. INTRODUCTION

Reactions induced by α particles play a significant role in the study of nuclear structure, nuclear reactions, and astrophysics. Reaction rate estimates within the framework of the Hauser-Feshbach (HF) statistical model must be further tested in order to validate the existing α -nucleus optical model potentials, especially at low energies, far below the Coulomb barrier. In addition, α -particle induced reactions are quite important to estimate significant effects for nuclear engineering design of fusion test facilities and accelerator-driven systems (ADS). Also, at low incident energies, α -induced reactions are important for nuclear astrophysics estimates.

The proton-rich nuclei heavier than Fe (the so-called p -process nuclei) are produced by a combination of (γ,n) , (γ,p) , and (γ,α) reactions on existing s or r nuclei at temperatures around a few GK, specific for explosive environments. In order to completely describe the p process a large reaction database involving thousands of reaction rates is necessary. The main problems encountered in the description of the p process of stellar nucleosynthesis were discussed by Arnould and Goriely [1]. In most of the cases the astrophysical rates were calculated by means of the HF model and the large discrepancies between experimental data and theoretical HF predictions observed in the case of α -capture reactions were interpreted as a result of the use of inappropriate α -potential models [2]. In the case of (γ,α) rates at astrophysical temperatures, determined via direct measurements or via inverse (α,γ) measurements, the α -nucleus optical potential is required in order to calculate the transmission probability of the α particle through the Coulomb barrier of the nucleus and, therefore, has a large impact on the calculated rates. Several potential parameters may have significant energy dependence across the Coulomb barrier. Therefore it is important to have as many data

as possible within this energy range. Recently, Rauscher [3] highlighted the astrophysical energy windows and the related experimental cross section measurements needed for further theoretical improvements of reaction rates (see Table I of [3]). Furthermore, there is a considerable lack of experimental data on the relevant cross sections in the p -process energy range, due to the fact that the direct measurement of most γ induced reactions is very difficult [4]. To overcome this difficulty, the charged particle induced reaction cross sections are measured and their inverse photodisintegration reaction cross sections are calculated using the detailed balance theorem [5]. Unfortunately the experimental data for charged particle induced reaction cross sections are also scarce for nuclei with $Z > 28$ because the energies of α -capture reactions relevant for nuclear astrophysics are well below the Coulomb barrier. This implies very small values for the cross sections and consequently are more difficult to measure. The (p,γ) measurements generally agree with the statistical model prediction within a factor of 2. For the (α,γ) case, one of the main problems for the calculation of reaction rates is the determination of the optical α -nucleus potentials at low energies (see Refs. [6–10] and references therein). The experimental studies indicate deviations of up to one order of magnitude of the HF predictions for α -capture and their inverse photodisintegration processes [2]. Therefore, it is important to investigate the α -induced reaction cross sections experimentally in order to test the reliability of the statistical model predictions.

Our experimental inquiry was also triggered by the fact that the stellar abundance of ^{115}Sn is underestimated by the s -process calculations [11]. More precisely, it is estimated that the s and r processes can account only for 50% of ^{115}Sn abundance [12] while recent p -process calculations cannot explain the remaining fraction [13,14]. In this respect, the measurement of the (α,γ) cross sections of this proton rich Sn isotope gives insights on the (γ,α) cross sections and implicitly on the dilemma involving the p -process contribution to the formation of proton rich Sn isotopes. Because the level density

* filipescu@tandem.nipne.ro

decreases at closed shells, the reactions on Sn isotopes are also good test candidates for the statistical model assumptions in the stellar process energy range.

Finally, extended experimental cross section data on Sn isotopes give a higher reliability in using global optical model parametrizations. Up to now experimental α -induced cross section are available on ^{112}Sn [15,16] and ^{117}Sn [17]. This work presents cross section measurements for the (α, γ) , (α, n) reactions on ^{115}Sn and (α, n) on ^{116}Sn , at incident beam energies between 9.6 and 15.3 MeV. It continues the work presented in [17] and will be extended with future measurements of α -induced cross sections at energies relevant for nuclear astrophysics for other Sn isotopes.

II. EXPERIMENT

Two target stack activation experiments were performed using $^4\text{He}^{2+}$ beams delivered by the Bucharest FN Tandem accelerator. Enriched tin self-supporting foils of $\sim 3.725 \text{ mg/cm}^2$ having 51.2% ^{115}Sn and 24.4% ^{116}Sn isotopic abundances were used in the first experiment. Due to the fact that the target was not mono-isotopic, ^{119}Te in both ground and isomeric states was created through two different reactions, with contributions depending on the cross sections and abundances. In order to disentangle the experimental cross section contributions due to the $^{115}\text{Sn}(\alpha, \gamma)^{119}\text{Te}$ and $^{116}\text{Sn}(\alpha, n)^{119}\text{Te}$ reactions, highly enriched ^{116}Sn targets (isotopic abundance $> 99\%$) were irradiated in a second experiment.

A. Target preparation

In the first experiment, the targets were mounted together in a stack having five tin layers alternating with aluminum foils (the first three of $10 \mu\text{m}$ thickness, and the last two of $2 \mu\text{m}$). The aluminum foils served as α -beam energy degraders and also as catchers for recoil nuclei from the Sn foils used for estimating the recoil fraction. The stack was irradiated with a 15.6 MeV $^4\text{He}^{2+}$ beam, such as to cover an energy range between 9.6 and 15.3 MeV, close to the Gamow peak energy of 8.6 MeV for the $^{115}\text{Sn}(\alpha, \gamma)^{119}\text{Te}$ reaction.

During the second experiment, two ^{116}Sn targets were mounted together with $10 \mu\text{m}$ Al spacers and a titanium foil of $6.7 \mu\text{m}$ placed at the end. The ^{116}Sn stack was irradiated two times at 15.6 MeV and 12.5 MeV incident energy respectively, with a 25 d cooling down time between irradiations. The α beam incident energies were adequately chosen such as to ensure mean irradiation energies inside the ^{116}Sn foils as close as possible to those from the first experiment. Remanent activity corrections were performed for the second irradiation.

In both experiments, the stacks were mounted into a Faraday cup, isolated from the rest of the beam line. A guard ring was placed at the Faraday cup entrance having a -300 V bias voltage in order to suppress the escape of the secondary electrons. The beam intensity was recorded in real time, in steps of one second, using an ORTEC 439 digital current integrator. The time dependence of the beam current recorded in the first experiment is presented in Fig. 1. In order to check the accuracy of the absolute values given by the current

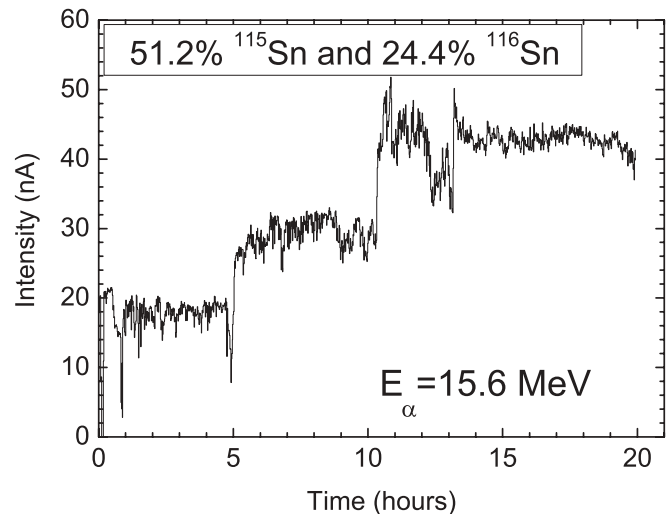


FIG. 1. Time dependence of beam intensity monitored in the first experiment.

integrator, the $^{48}\text{Ti}(\alpha, n)^{51}\text{Cr}$ cross section was also measured in the second experiment using the 320 keV γ ray emitted by ^{51}V , which resulted from EC decay of ^{51}Cr . The comparison between our results and the experimental data points of Morton *et al.* [18] and Baglin *et al.* [19] revealed a very good agreement.

The target thickness has an important role in this type of experiment, primarily because it occurs in the relations used for computing the cross section, but also because it defines the energy (and the energy spread) at which the cross sections are measured. For the purpose of determining the target thickness, besides weighing the targets, we made an additional α transmission measurement. The α source consisted of a mixture of ^{241}Am and ^{244}Cm . The energy spectra of the α particles transmitted through the Sn foils were measured with a totally depleted silicon detector. Target thicknesses were obtained by performing successive TRIM [20] simulations until we reproduced the attenuated energy spectrum, by considering the direct spectrum as input for the TRIM code.

B. Irradiations

The beam energies and straggling on the successive target foils were determined using the TRIM code. First, the simulated distributions of minimum, maximum, and medium energy of α particles in each foil were obtained. These distributions were then fitted with Gaussian functions to extract the mean values. Although the mean energy tends to be slightly different from the value obtained by averaging the minimum and maximum values, these two results are in agreement, considering the width of the Gaussian distribution. Finally, we adopted the mean value of the medium energy as the foil irradiation energy, while the minimum and maximum α particle energy distributions were used to obtain the energy range for each foil.

The characteristic α induced activity was measured with a pair of large volume ($\sim 55\%$ relative efficiency) HPGe detectors in close geometry to maximize the detection efficiency. The detectors were mounted in a low background

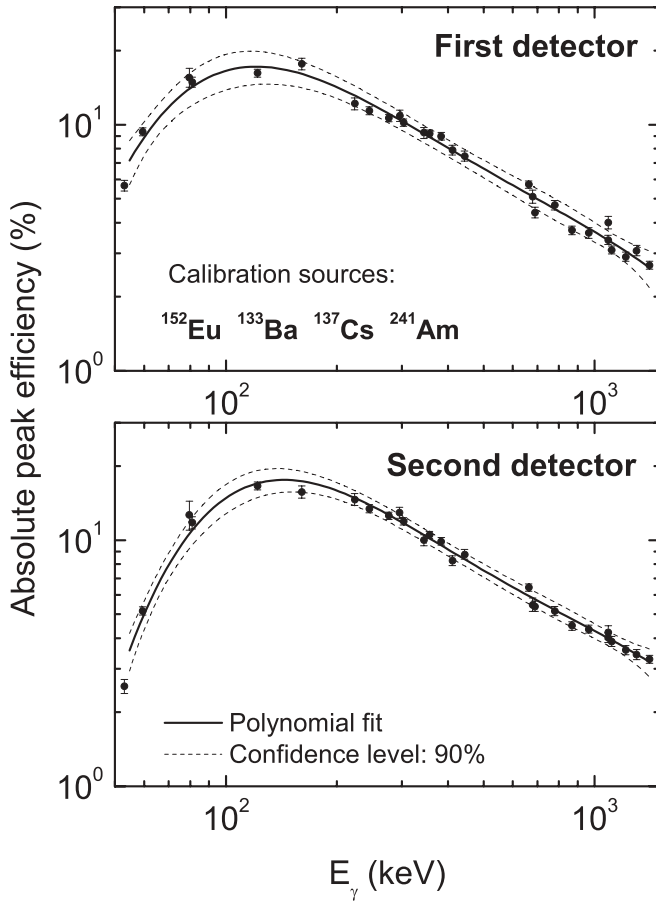


FIG. 2. Absolute peak efficiency for both detectors used in our experiment.

setup shielded with Pb walls and Cu and Al plates on the inside. A pulse generator with a fixed frequency for the output signal (20 Hz) was used for the dead-time correction. For the same purpose, we took into account the ^{40}K rate, as well as the dead-time indication of the data acquisition system. All three methods produced consistent results.

The efficiency calibration of HPGe detectors was done using calibrated point sources of ^{152}Eu , ^{133}Ba , ^{241}Am , and ^{137}Cs placed in the same geometry as the targets. Due to the close detection geometry the summing corrections were performed using the Monte Carlo simulation code GESPECOR [21]. The corrected calibration curves for each detector are presented in Fig. 2.

The activation technique involves bombarding a target with α particles to produce radioactive species and measurement of their specific activities after the irradiation has stopped. Details of the activation method and data analysis can be found in our previous papers [17,22,23].

C. γ -ray counting and analysis

During irradiation, ^{119}Te nuclei are obtained in both ground ($J^\pi = 1/2^+$, $T_{1/2} = 16.05$ d) and isomeric ($J^\pi = 11/2^-$, $T_{1/2} = 4.7$ d) states. The number N_M of nuclei populated in the isomeric state during irradiation has the following time

TABLE I. Irradiation energies in each foil obtained from TRIM [20] calculations.

1 st experiment 51.2% ^{115}Sn and 24.4% ^{116}Sn		2 nd experiment ^{116}Sn		
Foil #	Energy (MeV)		Foil #	Energy (MeV)
1	15.282 (318)	1 st	1	15.258 (342)
2	13.842 (332)	irradiation	2	13.751 (342)
3	12.298 (358)			
4	10.610 (390)	2 nd	1	12.108 (392)
5	9.596 (415)	irradiation	2	10.321 (411)

dependence:

$$\frac{dN_M}{dt} = \sigma_M \Phi(t) N_T - \lambda_M N_M(t), \quad (1)$$

where σ_M is the partial capture cross sections to the isomeric state, λ_M is the corresponding decay constant, and $\Phi(t)$ denotes the α beam flux at the irradiation time t . In this equation, we made the assumption that the number of target nuclei N_T does not vary significantly during the irradiation time, which is valid if the condition $\sigma \Phi \ll 1$ is satisfied.

By integrating the previous equation the total number of nuclei populated on the isomeric state at the end of the irradiation time t_a can be obtained as

$$N_M(t_a) = \sigma_M \rho h \frac{N_A}{\bar{A}_T} p e^{-\lambda_M t_a} \int_0^{t_a} e^{\lambda_M t} \frac{I(t)}{Z_p e} dt, \quad (2)$$

where p is the isotopic enrichment of the target, ρh is the target's specific thickness, N_A is the Avogadro number, Z_p is the projectile atomic number, \bar{A}_T is the target mean mass number, e is the electron charge, and $I(t)$ is the electrical beam intensity.

If the target is measured after a waiting time t_w , over the measuring time t_m , the following number of ^{119}Te nuclei will decay from the isomeric state:

$$N_M^{\text{dis}}(t_w, t_m) = N_M^i e^{-\lambda_M t_w} (1 - e^{-\lambda_M t_m}) \quad (3)$$

with N_M^i obtained from Eq. (3).

TABLE II. Nuclear data used to obtain experimental (α, γ) and (α, n) cross sections [39].

Nuclear reaction	E_x (keV)	J^π	$T_{1/2}$ (d)	E_γ (keV)	I_γ (%)
$^{115}\text{Sn}(\alpha, \gamma)^{119}\text{Te}^m$	260.96	11/2 ⁻	4.70(4)	153.59	66.2(3)
$^{116}\text{Sn}(\alpha, n)^{119}\text{Te}^m$				270.53	28.0(5)
				1212.73	66.2(3)
$^{115}\text{Sn}(\alpha, \gamma)^{119}\text{Te}^{\text{g.s.}}$	0.0	1/2 ⁺	0.669(2)	644.01	84.0(5)
$^{116}\text{Sn}(\alpha, n)^{119}\text{Te}^{\text{g.s.}}$				699.85	10.1(6)
$^{115}\text{Sn}(\alpha, n)^{118}\text{Te}$	0.0	0 ⁺	6.00(2)	1229.33	2.5(3)

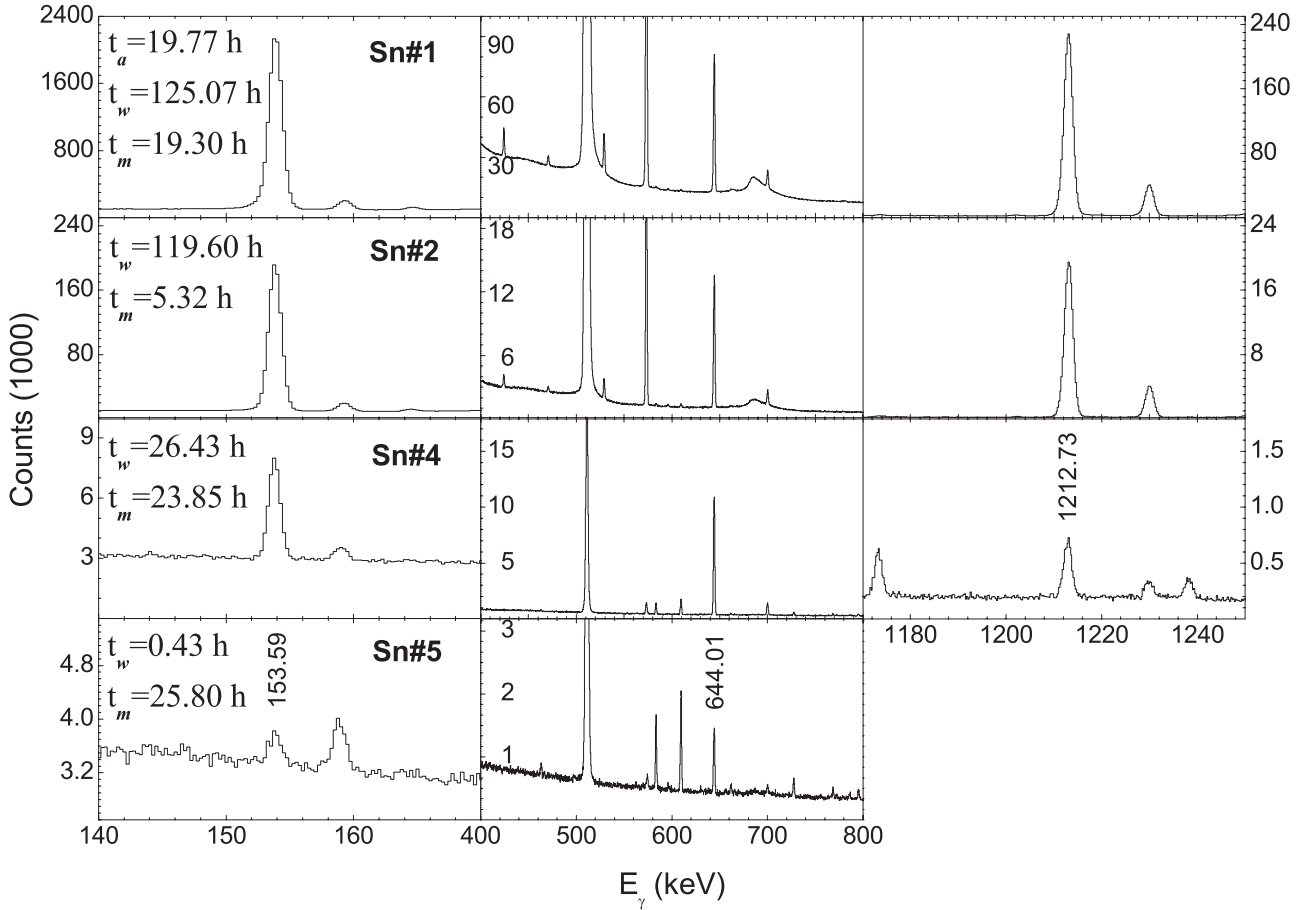


FIG. 3. Relevant parts of the HPGe γ -ray spectra measured in the first experiment. The transitions of interest for the determination of the cross section of the (α, γ) and (α, n) reactions on ^{115}Sn (Table II) are marked with their energy. The order numbers of the targets in the stack, the activation (t_a), waiting (t_w), and measuring (t_m) times are also indicated.

This number can be directly connected with the peak area A_i of a γ radiation γ_i , which is emitted only in the case of isomeric state decay

$$A_i = I_{\gamma_i} \varepsilon_i N_{M,G}^{\text{dis}}(t_w, t_m), \quad (4)$$

where ε_i represents the absolute peak efficiency for the γ_i radiation in the specified detection geometry, and I_{γ_i} is the absolute γ -ray intensity of the γ_i radiation.

The ground state of ^{119}Te is produced only by activation, because the isomeric state does not decay to the ground state, so the number of nuclei populating the ground state will be described by an expression similar with Eq. (3). Besides the population of ground and isomeric states of ^{119}Te through (α, γ) and (α, n) reactions on ^{115}Sn and ^{116}Sn , respectively, the ^{118}Te nucleus is also created through the $^{115}\text{Sn}(\alpha, n)$ reaction, and thus we could measure the cross section of this process using the same technique.

III. RESULTS AND DISCUSSION

A. Measured cross sections

The values of the irradiation energies obtained as explained in the previous section, together with the associated ranges, are given in Table I. For all these energies, except the lowest

one, both the $^{115}\text{Sn}(\alpha, \gamma)$ and $^{116}\text{Sn}(\alpha, n)$ channels were open and contributed together to the total production of ^{119}Te .

In the first experiment (target 51.2% ^{115}Sn /24.4% ^{116}Sn), for the last tin foil, irradiated at 9.6 MeV, only the $^{115}\text{Sn}(\alpha, \gamma)$ channel was opened, therefore we were able to measure one unaffected γ capture cross section for ^{115}Sn . For the other four mixed tin targets the $^{115}\text{Sn}(\alpha, \gamma)$ contribution was determined by analyzing the results of both experiments. The main nuclear data needed to obtain the cross sections are given in Table II.

Figure 3 displays some cuts from the γ -ray spectra obtained in the first experiment, indicating also the irradiation, waiting and counting times. Using these spectra, we obtained population cross sections of $^{119}\text{Te}^{\text{g.s.}}$, $^{119}\text{Te}^{\text{m}}$, and ^{118}Te for the target mentioned above (51.2% ^{115}Sn and 24.4% ^{116}Sn). These values, and the $^{116}\text{Sn}(\alpha, n)^{119}\text{Te}$ cross sections from the second experiment are given in Table III. It is worth mentioning that in the case of the first experiment, the following relations must be used for the population cross sections of the levels of interest:

$$\begin{aligned} \sigma_{\text{pop}}(^{119}\text{Te}^i) &= p_5 \sigma[^{115}\text{Sn}(\alpha, \gamma)^{119}\text{Te}^i] \\ &\quad + p_6 \sigma[^{116}\text{Sn}(\alpha, n)^{119}\text{Te}^i] \\ \sigma_{\text{pop}}(^{118}\text{Te}) &= p_5 \sigma[^{115}\text{Sn}(\alpha, n)^{118}\text{Te}], \end{aligned} \quad (5)$$

where p_5 and p_6 are the percentages of ^{115}Sn and ^{116}Sn in the targets, respectively.

TABLE III. Measured cross sections in present experiments (values are given in mb).

E_{α}^{Lab} (MeV)	$\sigma_{\text{pop}}(^{119}\text{Te}^{\text{g.s.}})$	1st experiment $\sigma_{\text{pop}}(^{119}\text{Te}^{\text{m}})$	$\sigma_{\text{pop}}(^{118}\text{Te})$
15.282 ± 0.318	47.46 ± 4.65	14.75 ± 1.30	73.69 ± 11.16
13.842 ± 0.332	16.15 ± 1.47	3.90 ± 0.34	23.48 ± 3.55
12.298 ± 0.358	2.16 ± 0.19	0.47 ± 0.04	3.22 ± 0.49
10.610 ± 0.390	0.071 ± 0.006	0.013 ± 0.001	0.11 ± 0.02
9.596 ± 0.415	$2.17 \times 10^{-3} \pm 2.24 \times 10^{-4}$	$8.53 \times 10^{-4} \pm 1.46 \times 10^{-4}$	
		2nd experiment	
	$\sigma[^{116}\text{Sn}(\alpha, n)^{119}\text{Te}^{\text{g.s.}}]$	$\sigma[^{116}\text{Sn}(\alpha, n)^{119}\text{Te}^{\text{m}}]$	
15.258 ± 0.342	149.19 ± 14.43	58.48 ± 5.53	
13.751 ± 0.342	54.77 ± 5.30	15.64 ± 1.48	
12.108 ± 0.392	3.62 ± 0.35	$0.85 \pm 0.28^{\text{a}}$	
10.321 ± 0.411	0.054 ± 0.005	$0.005 \pm 0.055^{\text{a}}$	
		Resulting experimental values	
	$\sigma[^{115}\text{Sn}(\alpha, \gamma)^{119}\text{Te}^{\text{g.s.}}]$	$\sigma[^{115}\text{Sn}(\alpha, \gamma)^{119}\text{Te}^{\text{m}}]$	$\sigma[^{115}\text{Sn}(\alpha, n)^{118}\text{Te}]$
15.282 ± 0.318	21.60 ± 15.96	$0.93 \pm 5.18^{\text{b}}$	143.93 ± 21.79
13.842 ± 0.332	5.45 ± 5.40	$0.16 \pm 1.38^{\text{b}}$	45.86 ± 6.94
12.298 ± 0.358	2.49 ± 0.55	0.52 ± 0.22	6.29 ± 0.95
10.610 ± 0.390	0.113 ± 0.015	0.023 ± 0.029	0.214 ± 0.035
9.596 ± 0.415	$4.24 \times 10^{-3} \pm 4.38 \times 10^{-4}$	$1.67 \times 10^{-3} \pm 2.85 \times 10^{-4}$	

^aErrors including remanent activity corrections.^bErrors due to dominant (α, n) channel at these energies.

In order to crosscheck the consistency of the population cross section ratios for the ground and isomeric states we made use of data from a previous experiment [24]. In this experiment, the Doppler shift attenuation method line shape analysis was used to measure lifetimes of excited states in ^{118}Te obtained by $^{115}\text{Sn}(\alpha, n)^{118}\text{Te}$ reaction. The same $^{115,116}\text{Sn}$ target as in the present experiment was irradiated with α particles of 15.3 MeV energy. The γ rays emitted following the reaction were detected in an array of seven HPGe detectors, while neutrons were detected with a one liter NE223 liquid scintillator detector. Using neutron gated spectra we were able to measure the relative intensities of the intense γ rays assigned to positive and negative parity bands (Table IV) in ^{119}Te . These additional experimental values were used to validate the choice of the high positive spin values for ^{119}Te , introduced in the statistical model (SM) calculations in order to describe the data above ~ 20 MeV. The details are given in the following section.

B. Comparison with model predictions

Recent studies of improved reaction rates for astrophysics [25–27] pointed out that an adequate description of the α +nucleus channel is still regarded as a current challenge in nuclear astrophysics. Statistical model predictions are overestimating the α -particle induced reaction cross sections below the Coulomb barrier by factors of 2–3 if the well-known

optical potential by McFadden and Satchler [28] is used. Therefore, in order to avoid possible compensation effects associated with the remaining parameters needed in SM calculations [29], we have used a consistent set of local SM parameters [30–33] established or validated on the basis of independent experimental information for, e.g., neutron total cross sections, γ -ray strength functions based on neutron-capture data, and low-lying level and resonance data.

The Koning and Delaroche [34] local neutron optical model potential (OMP) parameter set for the isotope ^{128}Te was adopted together with the use of Fermi-energy global values for each Te isotope. The global OMP of the same authors [34] was also considered for the calculation of the proton transmission coefficients on the Sb residual nuclei. A recent extension of the α -particle OMP [30] to all available

TABLE IV. The relative intensities of the strong γ rays assigned to positive and negative parity bands in ^{119}Te .

E_{γ} (keV)	E_i (keV)	J_i^{π}	E_f (keV)	J_f^{π}	Intensity (arb. units)
257.47	257.484	3/2 ⁺	0.0	1/2 ⁺	45505 (316)
320.39	320.506	5/2 ⁺	0.0	1/2 ⁺	16398 (274)
206.99	467.960	9/2 ⁻	260.96	11/2 ⁻	14809 (272)
240.13	501.10	7/2 ⁻	260.96	11/2 ⁻	9878 (248)
193.15	661.27	7/2 ⁻	467.96	9/2 ⁻	1342 (242)

α -particle induced reaction cross sections on nuclei within the mass number range $45 \leq A \leq 197$ below the Coulomb barrier provided a potential that describes also the α -particle elastic scattering at low energies [33]. This OMP (Table I of Ref. [33]) was used in the present SM calculations without any further tuning of the energy dependence of the real and/or imaginary potential depths [27]. Moreover, a systematic analysis of the neutron capture data for all stable isotopes of Sn and Te [35], for energies up to 3 MeV, was carried out. This was done in order to adopt a suitable normalization of the γ -ray strength functions $f_{E1}(\varepsilon_\gamma)$ given by the giant dipole resonance model with an energy-dependent Breit-Wigner (EDBW) line shape [36,37].

An updated version of the code STAPRE-H95 [38] was used to perform the calculations. The back-shifted Fermi gas (BSFG) formula was used for the nuclear level density at excitation energies below the neutron-separation energy, with the parameters a and Δ obtained by a fit of the recent experimental low-lying discrete levels [39] and s -wave nucleon resonance spacings D_0 [40]. The smooth-curve method was adopted [41] for nuclei without resonance data, to provide a values of the even-even, odd-odd, and odd-mass nuclei that were next kept fixed during the fit of low-lying discrete levels. The parameters used in the calculations are given in Table V together with the fitted data.

Consistent model calculations should reproduce the available data for all reaction channels and isotopes of an element. For this reason, our analysis included the earlier measured cross sections for the (α, n) and $(\alpha, 2n)$ reactions on ^{116}Sn for incident energies ≤ 30 MeV [42]. On the other hand, at the energies above 20–25 MeV the model calculations should consider the pre-equilibrium emission (PE) in addition to equilibrium decay of the remaining compound nucleus. A generalized geometry-dependent hybrid (GDH) model [43, 44] for PE processes which includes angular-momentum

conservation [45], and α -particle emission based on an α -particle preformation probability $\varphi = 0.2$ [46] was implemented in the STAPRE-H95 version of the original STAPRE-H95 code [47]. The same OMPs and nuclear level density parameters have been used in the framework of the OM, GDH, and HF models, for calculation of the intranuclear transition rates and single-particle level (s.p.l.) densities at the Fermi level [43,48,49].

The results of SM calculations using the above mentioned OMP parameters are shown in Fig. 4 for the (α, xn) total reaction cross sections of both target nuclei ^{115}Sn and ^{116}Sn . The figure also shows the SM results corresponding to the frequently used [25–27] OMPs of McFadden and Satchler [28] and Rauscher [50], with the remaining model parameters unchanged. The recent OMP [33] describes well the newly measured data, which cover six orders of magnitude. The previous potential Ref. [50] fails to describe the overall trend of the experimental data.

Once a rather suitable understanding of the α -particle OMP was obtained, we proceeded to analyze the measured (α, n) reaction cross sections to both the ground (g.s.) and the long-lived isomeric state of the residual nucleus ^{119}Te . The SM results are shown in Fig. 5(a) and 5(b). The experimental cross sections given in Table III are well described, with the exception of the ^{119}Te g.s. activation through the (α, γ) reaction on ^{115}Sn . Actually, even in the latter case there is an agreement within two standard deviations for the two values measured at the highest incident energies while those at lower energies are overestimated. Larger differences between experiment and model predictions are expected, in fact, at energies above 20 MeV [42], where PE effects on the calculated cross sections may be important. Results of PE + SM calculations are shown in Fig. 5(c) and 5(d), corresponding to a PE fraction of $\sim 20\%$ from the total reaction cross section at the incident energy of 30 MeV. One can see, first, that the cross sections no longer

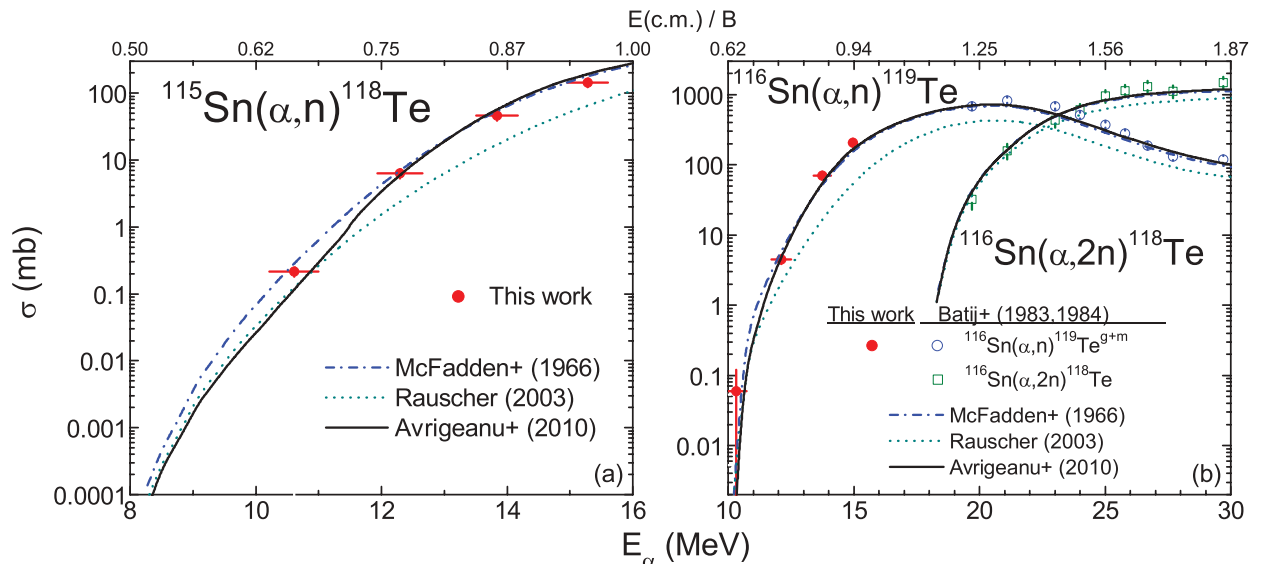


FIG. 4. (Color online) Comparison of measured (this work and Ref. [42]) and calculated (α, n) and $(\alpha, 2n)$ reaction cross sections for the target nuclei (a) ^{115}Sn and (b) ^{116}Sn , using the α -particle OMPs of Refs. [28] (dash-dotted curves), [50] (dotted), and [33] (solid).

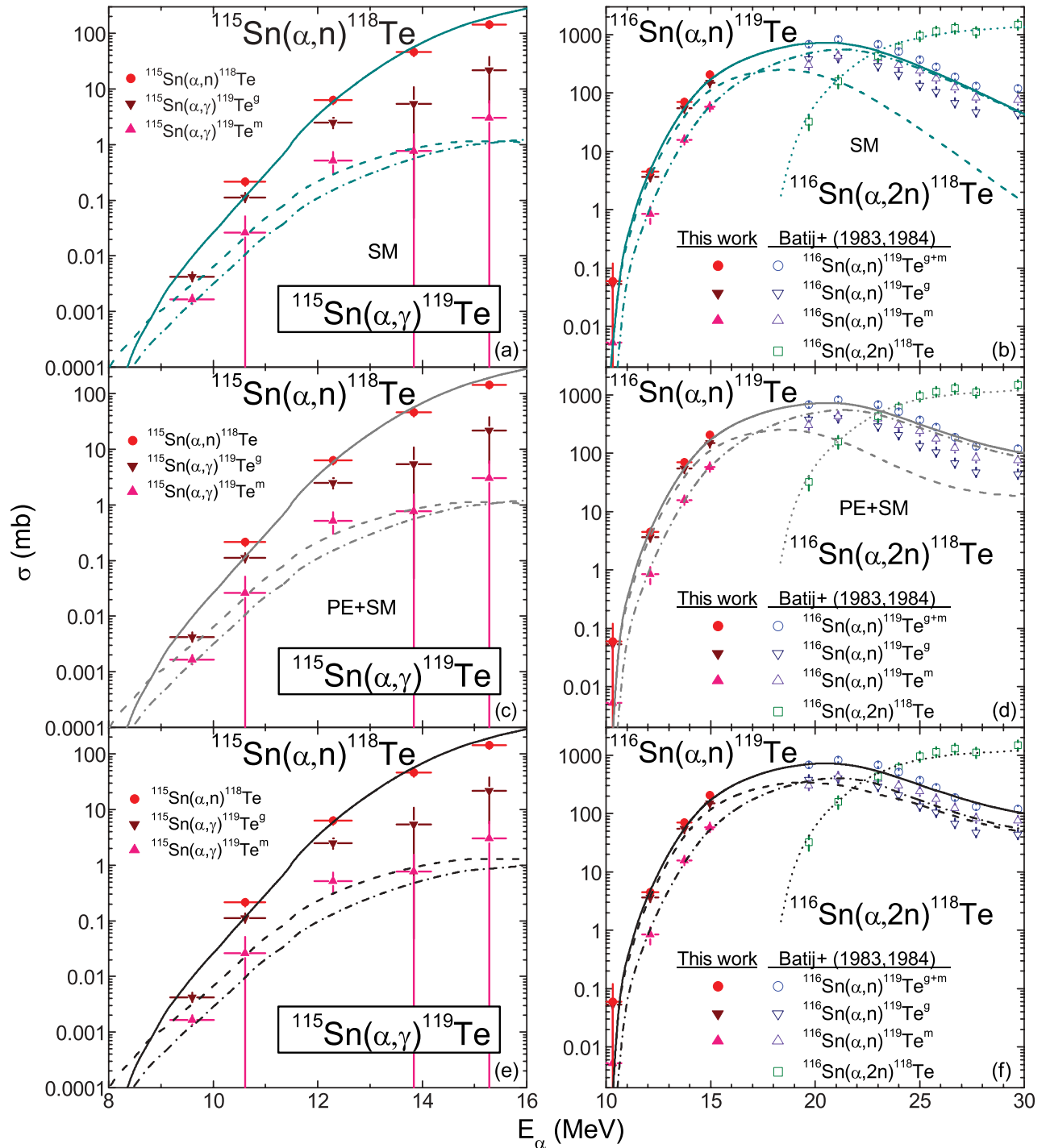


FIG. 5. (Color online) Comparison of measured (this work and Ref. [42]) and calculated (α,γ) , (α,n) and $(\alpha,2n)$ reaction total (solid curves) and partial cross sections to the ground (dashed curves) and isomeric (dash-dot curves) states of the residual nuclei, for the target nuclei (a,c,e) ^{115}Sn and (b,d,f) ^{116}Sn , using the α -particle OMPs of Ref. [33] within calculations based on the (a,b) statistical model (SM), (c,d) SM and PE model considering a $7/2^+$ spin for the excitation energies of levels at 906, 957, and 1093 keV, and (e,f) the same levels assumed as $11/2^+$, $13/2^+$, and $15/2^+$, respectively.

continue to decrease at the higher energies, and second, that the cross section for the g.s. and isomeric states increases by a factor between 2 and 10. Thus, inclusion of the PE brings the isomeric state cross sections into quite good agreement with the experimental data while those for the g.s. still remain

underpredicted by a factor of ~ 2 . No change of the PE + SM parameters proved able to reduce the disagreement for the g.s. cross sections. On the other hand, the agreement at incident energies below 15 MeV confirmed the input parameters used, the above mention disagreement being more likely related to

TABLE V. Low-lying level number N_d up to excitation energy E_d [39] used in the reaction cross-section SM calculations, and the levels and s -wave neutron-resonance spacings D_0^{exp} in the energy range ΔE above the separation energy S , for the target-nucleus g.s. spin I_0 , fitted to obtain the BSFG level-density parameter a and g.s. shift Δ (for a spin cutoff factor calculated with a variable moment of inertia between 50% and 75% of the rigid-body value, from g.s. to S , and reduced radius $r_0 = 1.25$ fm).

Nucleus	N_d	E_d (MeV)	Fitted level and resonance data					a (MeV ⁻¹)	Δ (MeV)
			N_d	E_d (MeV)	$S + \frac{\Delta E}{2}$ (MeV)	I_0	D_0^{exp} (keV)		
¹¹⁴ Sn	17	2.860	17	2.86				13.85	1.34
¹¹⁵ Sn	23	2.084	23	2.08	7.546	0	0.286(106)	13.75	0.40
¹¹⁶ Sn	26	3.105	26	3.11				13.45	1.33
¹¹⁷ Sb	17	1.536	17	1.54				14.10	0.05
¹¹⁸ Sb	6	0.166	6	0.17				14.00	-1.35
¹¹⁹ Sb	26	1.821	26	1.82				14.00	0.10
¹¹⁷ Te	8	0.681	8	0.68				13.80	-0.55
¹¹⁸ Te	24	2.422	24	2.42				14.00	0.75
¹¹⁹ Te	34	1.093	32	1.00				14.70	-0.70
¹²⁰ Te	20	2.461	20	2.46				14.00	0.87

spin assignments of low-lying levels. Thus, it is obvious that the probability distributions of the population of entry states in the (α, n) reaction around 15 and 30 MeV, are quite different. While the spins corresponding to the related maximum are $\sim 1\hbar$ (see Fig. 5 of Ref. [51]) in the former case, they are well above $10\hbar$ in the latter. As a consequence, higher-spin discrete levels are populated with increased probability for incident energies above ~ 20 MeV. The known low-lying level scheme of the residual nucleus ¹¹⁹Te, has a number of $N_d = 34$ levels up to the excitation energy $E_d = 1093$ keV (Table V) [52], including negative-parity levels up to spin $15/2$ that finally decay to the isomeric state, and positive-parity levels only up to spin $9/2$ finally feeding the g.s. In order to have levels with similar spins

for both parities, one should enlarge the number of discrete levels taken into account up to an excitation energy of about 3.4 MeV [52] but this is difficult to handle in the input of the SM code. In order to simulate the influence of positive parity levels of higher spin, we proceeded as follows. The levels with excitation energies of 906, 957, and 1093 keV, with no original spin assignment [52], were considered first as having a spin of $7/2^+$ in the calculations shown in Fig. 5(a) and 5(d). As levels with spin-parity values of $11/2^+$, $13/2^+$, and $15/2^+$ exist at excitation energies just a few hundreds of keV higher, we assumed, in a second calculation, the above mentioned spin values for the levels at 906, 957, and 1093 keV respectively, and also considered that the decays for these levels finally populate the $1/2^+$ g.s. The calculations performed with these two assumptions are shown in Fig. 5(e) and 5(f). An obvious improvement of both shape and absolute value of the (α, n) cross sections for both the g.s. and isomeric state is obtained over the whole energy range. Nevertheless, the above spin and parity assignments should be considered only as a tentative way to describe more realistically the ¹¹⁹Te continuum decay to the low-lying levels. With this observation, the final agreement of the calculated and measured cross sections for the ground and isomeric states of ¹¹⁹Te over more than six orders of magnitude confirm the accuracy and consistency of the SM + PE calculation.

Finally, the comparison between experimental values of relative γ -ray intensities of the intense γ rays assigned to positive and negative parity bands of ¹¹⁹Te (Table IV) and the results of SM+PE calculations are shown in Fig. 6. The good agreement emphasizes even more the need to explicitly consider higher spin values for the discrete levels in the positive parity band of ¹¹⁹Te, as already discussed within the above section.

IV. SUMMARY AND CONCLUSIONS

In a first experiment, the characteristic activity of both ground and isomeric states of ¹¹⁹Te was measured using an

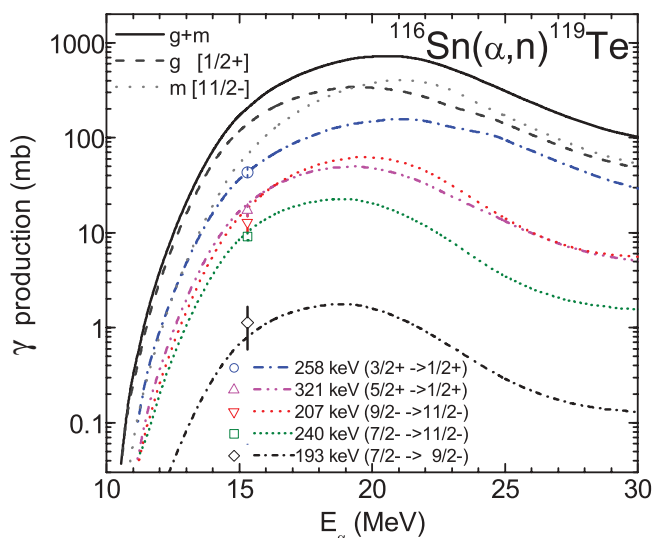


FIG. 6. (Color online) Comparison of measured (this work) and calculated excitation functions of the 258, 321, 207, 240, and 193 keV γ rays assigned to positive and negative parity bands in ¹¹⁹Te. A normalization to the calculated value of the 257 keV γ -ray intensity at the incident energy of 15.3 MeV has been used for the relative intensities given in Table IV.

enriched target of tin, with 51.2% ^{115}Sn and 24.4% ^{116}Sn isotopic abundances. Due to the fact that the target was not mono-isotopic, ^{119}Te in both ground and isomeric states was created through different reactions, with contributions depending of the cross sections and abundances. One data point was measured at an energy where only the $^{115}\text{Sn}(\alpha,\gamma)$ channel contributed to the production of ^{119}Te . The other four points were measured at energies where both $^{115}\text{Sn}(\alpha,\gamma)$ and $^{116}\text{Sn}(\alpha,n)$ channels are open and thus contributed together to the production of ^{119}Te . To disentangle the different contributions, highly enriched ^{116}Sn targets (isotopic abundance > 99%) were irradiated in a different experiment, at incident energies adequately chosen such as to ensure mean irradiation energies inside the ^{116}Sn foils as close as possible to the ones from the first experiment.

The results of pre-equilibrium and statistical-model calculations using a recent α -particle optical potential [33] are found to describe well the newly measured data, without any further tuning of, e.g., energy dependence of the real and/or imaginary parts.

Moreover, an obvious improvement of both shape and absolute value of (α, n) cross sections for both the g.s. and isomeric state over the whole energy range was obtained only after the assumption of spin values ($11/2^+$, $13/2^+$, and $15/2^+$) for some of the levels with no current spin

assignments [52] situated in the upper part of the discrete level scheme considered in the calculations. This artifice should be considered only as a way to illustrate the need for a better description of the ^{119}Te continuum decay to the low-lying levels. The final agreement of the calculated and measured cross sections for the ground and isomeric states of ^{119}Te over more than six orders of magnitude confirms the accuracy and consistency of the model calculations.

The theoretical evaluation still slightly underestimates the experimental cross sections. Therefore, one could make use of the present new experimental results to bring a valuable contribution to the determination of astrophysical rates. These results should also be of value in solving the puzzle concerning the origin of this rare tin isotope. Further measurements with a highly enriched ^{115}Sn target are deemed as very useful.

ACKNOWLEDGMENTS

We like to thank Dr. Mark Caprio for reading the paper and useful comments. This work was partly supported by the National Authority of the Scientific Research (ANCS) under project nos. PN-09-37-01-05, CNCSIS-UEFISCSU-ID-362 48/28.09.2007, 24EU-ISOLDE/2009, and PNCDI-II 71-051 RIHAD.

-
- [1] M. Arnould and S. Goriely, *Phys. Rep.* **384**, 1 (2003).
 [2] W. Rapp, J. Görres, M. Wiescher, H. Schatz, and F. Käppeler, *Astrophys. J.* **653**, 474 (2006).
 [3] T. Rauscher, *Phys. Rev. C* **81**, 045807 (2010).
 [4] H. Utsunomiya, P. Mohr, A. Zilges, and M. Rayet, *Nucl. Phys. A* **777**, 459 (2006).
 [5] C. Angulo *et al.*, *Nucl. Phys. A* **656**, 3 (1999).
 [6] E. Somorjai *et al.*, *Astron. Astrophys.* **333**, 1112 (1998).
 [7] Gy. Gyürky, Zs. Fülöp, E. Somorjai, M. Kokkoris, S. Galanopoulos, P. Demetriou, S. Harissopulos, T. Rauscher, and S. Goriely, *Phys. Rev. C* **68**, 055803 (2003).
 [8] Gy. Gyürky, Zs. Fülöp, and E. Somorjai, *Nucl. Phys. A* **758**, 90c (2005).
 [9] P. Descouvemont and T. Rauscher, *Nucl. Phys. A* **777**, 137 (2006).
 [10] T. Rauscher, *Phys. Rev. C* **73**, 015804 (2006).
 [11] C. Arlandini, F. Käppeler, K. Wisshak, R. Gallino, M. Lugaro, M. Busso, and O. Straniero, *Astrophys. J.* **525**, 886 (1999).
 [12] K. Wisshak, F. Voss, Ch. Theis, F. Käppeler, K. Guber, L. Kazakov, N. Kornilov, and G. Reffo, *Phys. Rev. C* **54**, 1451 (1996).
 [13] N. Prantzos, M. Hashimoto, M. Rayet, and M. Arnould, *Astron. Astrophys.* **238**, 455 (1990).
 [14] W. Howard, B. Meyer, and S. Woosley, *Astrophys. J.* **373**, L5 (1991).
 [15] N. Özkan *et al.*, *Phys. Rev. C* **75**, 025801 (2007).
 [16] W. Rapp *et al.*, *Phys. Rev. C* **78**, 025804 (2008).
 [17] Căta-Danil *et al.*, *Phys. Rev. C* **78**, 035803 (2008).
 [18] A. J. Morton, S. G. Tims, A. F. Scott, V. Y. Hansper, C. I. W. Tingwell, and D. G. Sargood, *Nucl. Phys. A* **537**, 167 (1992).
 [19] C. M. Baglin, E. R. Norman, R. M. Larimer, and G. A. Rech, *AIP Conf. Proc.* **769**, 1370 (2005).
 [20] J. F. Ziegler, J. P. Biersack, and U. Littmark, *The Stopping and Range of Ions in Solids* (Pergamon Press, New York, 1985).
 [21] O. Sima, D. Arnold, and C. Dovlete, *J. Radioanal. Nucl. Chem.* **248**, 359 (2001).
 [22] I. Căta-Danil *et al.*, *Rom. Rep. Phys.* **59**, 177 (2007).
 [23] I. Căta-Danil *et al.*, *Rom. Rep. Phys.* **60**, 555 (2008).
 [24] C. Mihai *et al.*, *Phys. Rev. C* **83**, 054310 (2011).
 [25] C. Yalçın *et al.*, *Phys. Rev. C* **79**, 065801 (2009).
 [26] Gy. Gyürky *et al.*, *J. Phys. G: Nucl. Part. Phys.* **37**, 115201 (2010).
 [27] T. Rauscher, *Int. J. Mod. Phys. E* (in press); [<http://www.arxiv.com/pdf/1010.4283v1>].
 [28] L. McFadden and G. R. Satchler, *Nucl. Phys. A* **84**, 177 (1966).
 [29] P. Demetriou, C. Grama, and S. Goriely, *Nucl. Phys. A* **707**, 253 (2002).
 [30] M. Avrigeanu, A. C. Obreja, F. L. Roman, V. Avrigeanu, and W. von Oertzen, *At. Data Nucl. Data Tables* **95**, 501 (2009); [arXiv:0808.0566v1](http://arxiv.org/pdf/0808.0566v1) [<http://arxiv.org/pdf/0808.0566v1>].
 [31] M. Avrigeanu and V. Avrigeanu, *Phys. Rev. C* **79**, 027601 (2009).
 [32] M. Avrigeanu and V. Avrigeanu, *Phys. Rev. C* **81**, 038801 (2010).
 [33] M. Avrigeanu and V. Avrigeanu, *Phys. Rev. C* **82**, 014606 (2010).
 [34] A. J. Koning and J. P. Delaroche, *Nucl. Phys. A* **713**, 231 (2003).
 [35] V. Avrigeanu, F. L. Roman, and M. Avrigeanu, in *Proc. 4th NEMEA-4 Workshop on Neutron Measurements, Evaluations and Applications, Prague, Czechia (2007)*, edited by A. Plompen, European Commission Report EUR 23235 EN, Belgium, 2008, p. 143; [<http://www.irmm.jrc.be/html/publications/>].

- [36] D. G. Gardner and F. S. Dietrich, Report Lawrence Livermore National Laboratory UCRL-82998, Livermore, 1979.
- [37] M. Avrigeanu, V. Avrigeanu, G. Căta, and M. Ivascu, *Rev. Roum. Phys.* **32**, 837 (1987).
- [38] M. Avrigeanu and V. Avrigeanu, IPNE Report NP-86-1995, Bucharest, 1995, and Refs. therein; *News NEA Data Bank* **17**, 22 (1995).
- [39] Evaluated Nuclear Structure Data File (ENSDF), [www.nndc.bnl.gov/ensdf/].
- [40] R. Capote *et al.*, *Nucl. Data Sheets* **110**, 3107 (2009); [<http://www-nds.iaea.org/RIPL-3/>].
- [41] C. H. Johnson, *Phys. Rev. C* **16**, 2238 (1977).
- [42] V. G. Batij *et al.*, EXFOR Nuclear Reaction Data file A0203, dated 1983-12-14; EXFOR Nuclear Reaction Data file A0217, dated 1984-05-21; [<http://www-nds.iaea.or.at/exfor/>].
- [43] M. Blann, *Nucl. Phys. A* **213**, 570 (1973).
- [44] M. Blann and H. K. Vonach, *Phys. Rev. C* **28**, 1475 (1983).
- [45] M. Avrigeanu, M. Ivascu, and V. Avrigeanu, *Z. Phys. A* **329**, 177 (1988); **335**, 299 (1990).
- [46] E. Gadioli and E. Gadioli-Erba, *Z. Phys. A* **299**, 1 (1981).
- [47] M. Uhl and B. Strohmaier, Report IRK-76/01, IRK, Vienna, 1981.
- [48] M. Avrigeanu and V. Avrigeanu, *J. Phys. G: Nucl. Part. Phys.* **20**, 613 (1994).
- [49] M. Avrigeanu and V. Avrigeanu, *Comput. Phys. Commun.* **112**, 191 (1998); A. Harangozo, I. Stetcu, M. Avrigeanu, and V. Avrigeanu, *Phys. Rev. C* **58**, 295 (1998).
- [50] T. Rauscher, *Nucl. Phys. A* **719**, 73c (2003); **725**, 295(E) (2003).
- [51] C. Mihai *et al.*, *Phys. Rev. C* **81**, 034314 (2010).
- [52] D. M. Symochko, E. Browne, and J. K. Tuli, *Nucl. Data Sheets* **110**, 2945 (2009).